LETTERS
PUBLISHED ONLINE: 1 APRIL 2012 | DOI: 10.1038/NMAT3292
nature materials

Gradient-index meta-surfaces as a bridge linking propagating waves and surface waves

Shulin Sun[1,2†], Qiong He[1†], Shiyi Xiao[1†], Qin Xu[1], Xin Li[1] and Lei Zhou[1*]

The arbitrary control of electromagnetic waves is a key aim of photonic research. Although, for example, the control of freely propagating waves (PWs; refs 1–6) and surface waves (SWs; refs 7–10) has separately become possible using transformation optics and metamaterials, a bridge linking both propagation types has not yet been found. Such a device has particular relevance given the many schemes of controlling electromagnetic waves at surfaces and interfaces, leading to trapped rainbows[11,12], lensing[13–16], beam bending[17], deflection[18–20], and even anomalous reflection/refraction[21,22]. Here, we demonstrate theoretically and experimentally that a specific gradient-index meta-surface can convert a PW to a SW with nearly 100% efficiency. Distinct from conventional devices such as prism[23] or grating[24–26] couplers, the momentum mismatch between PW and SW is compensated by the reflection-phase gradient of the meta-surface, and a nearly perfect PW–SW conversion can happen for any incidence angle larger than a critical value. Experiments in the microwave region, including both far-field and near-field characterizations, are in excellent agreement with full-wave simulations. Our findings may pave the way for many applications, including high-efficiency surface plasmon couplers, anti-reflection surfaces, light absorbers, and so on.

SW, a special type of electromagnetic (EM) wave bounded at a metal/dielectric interface often coupled with charge oscillations[27], has a parallel $\mathbf{k}$ vector larger than $k_0=\omega/c$ (ω is the wavelength and c is the light speed in medium) possessed by a PW. Snell's law prevents a direct conversion between a PW and a SW at a flat interface owing to the momentum mismatch[28]. Our idea on PW–SW conversion is inspired by examining the radiation characteristics of a charge density wave (CDW; ref. 29), which itself is a part of a SW. As shown in Fig. 1a, consider a surface current $\mathbf{j}(\mathbf{r},t)=J_0 e^{i\xi x}e^{-i\omega t}\delta(z)\hat{\mathbf{x}}$ generated on the x–y plane at $z=0$, which corresponds to a charge distribution $\rho(x,t)=(\xi J_0/\omega)e^{i\xi x}e^{-i\omega t}\delta(z)$ describing (effectively) a collection of charges moving at velocity $v_e=\omega/\xi$. The radiation pattern of such a current sheet can be obtained by solving the Maxwell equations, yielding an exact solution

$$\mathbf{E}(\mathbf{r},t)=(\mu_0 J_0 c/2k_0)\cdot\left(-\sqrt{k_0^2-\xi^2}\,\hat{\mathbf{x}}+\xi\hat{\mathbf{z}}\right)e^{i\xi x}e^{i\sqrt{k_0^2-\xi^2}z}e^{-i\omega t} \quad (1)$$

in the region $z>0$ (see Supplementary Information). Clearly, the radiated wave is a PW when $\xi<k_0$, but becomes a SW when $\xi>k_0$, indicating that ξ is a crucial parameter to dictate the nature of radiation. Intuitively, these results can be understood by making an analogy with Cherenkov radiation[30]. Given that the effective velocity is $v_e=\omega/\xi$ for the moving charges, the condition $\xi<k_0$ ($\xi>k_0$) is equivalent to $v_e>c$ ($v_e<c$), consistent with the Cherenkov effect that the radiation to free space for a moving charge is only possible when $v_e>c$ (ref. 30).

Understanding these results help us design a PW–SW converter. As shown in Fig. 1b, the problem is equivalent to finding such a system, when illuminated by an incident PW, that its generated electric current is $\mathbf{j}=\mathbf{J}_0 e^{i\xi x}e^{-i\omega t}\delta(z)$ with $\xi>k_0$. Suppose the incident PW is $\mathbf{E}_{in}=E_0 e^{i(-k_0 z-\omega t)}\hat{\mathbf{x}}$, obviously, a flat metal sheet does not work because the induced current is uniform. However, if we cap the metal sheet with a metamaterial (MM) slab with non-uniform $\varepsilon_M(x)$ and $\mu_M(x)$, the current $\mathbf{j}(x,z)e^{-i\omega t}$ generated inside the entire structure (MM + metal) is highly inhomogeneous. Assuming $d\ll\lambda$, where d and λ are the MM slab thickness and the working wavelength, we can integrate $\mathbf{j}(x,z)$ over the thickness d to define an effective surface current: $\mathbf{J}_{eff}(x)=\int\mathbf{j}(x,z)\,dz$. Therefore, if the MM layer is designed such that its induced surface current is $\mathbf{J}_{eff}(x)=J_0 e^{i\xi x}\hat{\mathbf{x}}$ when illuminated by an incident PW, the EM wave radiated from the system must carry a parallel $\mathbf{k}$ vector, $k_x=\xi$, according to equation (1), and when $\xi>k_0$, the incident PW is then perfectly converted to a SW bounded by the surface.

To determine the properties of the MM slab (that is, $\varepsilon_M(x)$, $\mu_M(x)$ and d), we assume that $\mathbf{J}_{eff}(x_0)$ at a particular point x_0 can be approximated by $\mathbf{J}^0_{eff}$ generated on a model system where the MM is replaced by a homogeneous slab with $\varepsilon=\varepsilon_M(x_0)$, $\mu=\mu_M(x_0)$. With a perfect electric conductor (PEC) on the back, the system (that is, homogeneous MM + PEC) is always perfectly reflecting so that the reflected $\mathbf{E}$ field can be written as $\mathbf{E}_r=e^{i\Phi}E_{in}e^{i(k_0 z-\omega t)}\hat{\mathbf{x}}$ with Φ given by

$$\Phi=\cos^{-1}\left\{\left[-\varepsilon+\mu\tan^2(\sqrt{\varepsilon\mu}k_0 d)\right]/\left[\varepsilon+\mu\tan^2(\sqrt{\varepsilon\mu}k_0 d)\right]\right\} \quad (2)$$

As the reflected wave is generated by the surface current, $\mathbf{E}_r$ must be a linear function of $\mathbf{J}^0_{eff}$, so that $\mathbf{J}^0_{eff}$ must take the same phase as $\mathbf{E}_r$, $\mathbf{J}^0_{eff}=\hat{\mathbf{x}}J_0 e^{i\Phi}$. Thus, the effective surface current on the meta-surface must be $\mathbf{J}_{eff}(x)=\mathbf{J}_0 e^{i\Phi(x)}$, where $\Phi(x)$ describes the (local) reflection phase measured at the point x, calculated by equation (2) with $\varepsilon=\varepsilon_M(x)$, $\mu=\mu_M(x)$. Therefore, the MM should be designed such that

$$\Phi(x)=\Phi_0+\xi x \quad (\text{with } \xi>k_0) \quad (3)$$

for the entire system to work as a PW–SW converter. Equations (2) and (3) are the key for the design. The simplest solution of equations (2) and (3) is $\varepsilon_M(x)=\mu_M(x)=1+\xi x/2k_0 d$. Other more practical designs include the $[\varepsilon_M(x)=\text{const.},\mu_M(x)]$ and $[\varepsilon_M(x),\mu_M(x)=\text{const.}]$ models. In the present case, assuming

[1]State Key Laboratory of Surface Physics, Key Laboratory of Micro and Nano Photonic Structures (Ministry of Education) and Physics Department, Fudan University, Shanghai 200433, China, [2]National Center of Theoretical Sciences at Taipei (Physics Division) and Department of Physics, National Taiwan University, Taipei 10617, Taiwan. †These authors contributed equally to this work. *e-mail: phzhou@fudan.edu.cn.

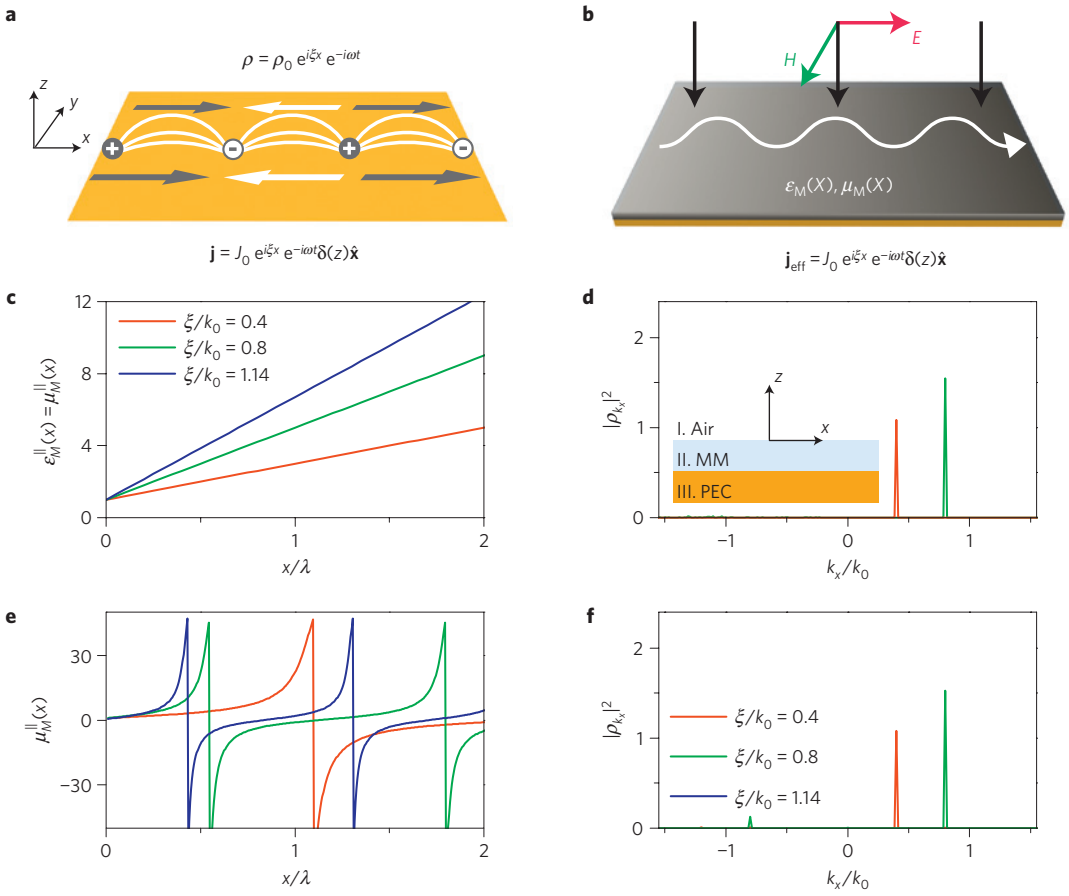

Figure 1 | Physical concept of the PW–SW conversion and mode-expansion calculations on model systems. a, A surface current $\mathbf{j} = J_0 e^{i\xi x} e^{-i\omega t}\delta(z)\hat{\mathbf{x}}$ can generate a PW or a SW depending on the value of ξ/k_0. **b**, A meta-surface combining a thin gradient-index MM layer with a perfect electric conductor (PEC) can generate an effective current $\mathbf{j}_{eff} \approx J_0 e^{i\xi x} e^{-i\omega t}\delta(z)$ under illumination of an incident PW, so as to convert the PW to a SW if $\xi > k_0$. **c**,**e**, For three meta-surfaces with different ξ/k_0 designed based on two models (**c**,**e**) their $\varepsilon_M^{\parallel}(x), \mu_M^{\parallel}(x)$ distributions (assuming $\varepsilon_M^z(x) = \mu_M^z(x) = 1$). **d**,**f**, Scattering coefficients $|\rho_{k_x}|^2$ versus k_x for meta-surfaces with $\xi < k_0$, calculated when the meta-surfaces are illuminated by a normally incident *x*-polarized PW. Here **c** and **d** are based on the $[\varepsilon_M^{\parallel}(x) = \mu_M^{\parallel}(x)]$ model and **e** and **f** are based on the $[\varepsilon = 1, \mu_M^{\parallel}(x)]$ model, and the thicknesses of the MM layers are $d = \lambda/20$.

normal incidence, the z components of ε_M and μ_M are not important. Therefore, one can also let only $\varepsilon_M^{\parallel}$ and/or $\mu_M^{\parallel}$ to vary as functions of x, yielding more solutions, which are helpful in practical designs. Figure 1c and e explicitly show three solutions of equations (2) and (3) based on the $\varepsilon_M^{\parallel} = \mu_M^{\parallel}$ and $[\varepsilon = 1, \mu_M^{\parallel}(x)]$ models, adopting three typical ξ values. As ε and μ can not be infinitely large in realistic samples, we purposely introduced super cells to make ε and μ fall into an experimentally realizable range. We note that introducing super cells does not affect the main physics here (see Supplementary Information).

To justify the approximation adopted in deriving equations (2) and (3), we developed a rigorous mode-expansion theory[31,32] to study the EM wave scattering of our gradient-index systems. As shown in the inset in Fig. 1d, we divide the entire space into three regions. EM eigenmodes in region I are plane waves denoted by $\mathbf{E}_I^0(\sigma, k_x)$ characterized by the polarization σ and k_x. In region II, we numerically solved the Maxwell equations to obtain a series of eigenmodes. We then expanded EM fields as linear combinations of eigenmodes in different regions and determined all the expansion coefficients by matching the boundary conditions at the two interfaces. Assuming that the incident wave is p-polarized with an incident angle θ_i, we found the scattered $\mathbf{E}$ field contains only p-polarized waves and can be written as $\mathbf{E} = \sum_{k_x} \rho_{k_x} \mathbf{E}_I^0(p, k_x)$, with ρ_{k_x} being the expansion coefficient for the eigenmode $\mathbf{E}_I^0(p, k_x)$ inside the diffracted beam (see Supplementary Information). We applied the theory to study the scattering problem for model systems with $\xi < k_0$, as described in Fig. 1c and e, and show the calculated $|\rho_{k_x}|^2$ spectra (setting $\theta_i = 0°$) in Fig. 1d and f, respectively. For both types of model, we found $|\rho_{k_x}|^2$ to be significantly enhanced at $k_x = \xi$ and nearly zero elsewhere, justifying our previous arguments (see Supplementary Information for the energy conversion efficiency). The mode-expansion calculations on infinitely large $\xi > k_0$ systems cannot identify the PW–SW conversion efficiencies, because the input PW takes an infinite energy whereas the outgoing SW always takes a finite energy. Numerical calculations performed on a finite $\varepsilon = \mu$ and $\xi = 1.14k_0$ system verify that nearly all the incoming energy of the input PW is converted to that of a SW with $k_x = \xi$ bounded on the $\xi = 1.14k_0$ meta-surface, justifying our theoretical conjecture (see Supplementary Information). Extending to the oblique incidence case where an additional parallel $\mathbf{k}$ vector, $k_x^0 = k_0 sin\theta_i$, is provided by the input beam, we found that the parallel wave vector of the reflected beam must be

$$k_x = \xi + k_0 \sin\theta_i \tag{4}$$

Equation (4) states that, for any PW, one can always design a gradient-index meta-surface with an appropriate ξ and select an appropriate incidence angle θ_i to couple the PW completely into a SW bounded on the meta-surface. Therefore, such a system is the desired bridge between PW and SW, with ξ and θ_i as two crucial parameters to control their linkage. We note that equation (4) recovers the generalized Snell's law recently discovered[21,22] in the case of $k_x, \xi < k_0$

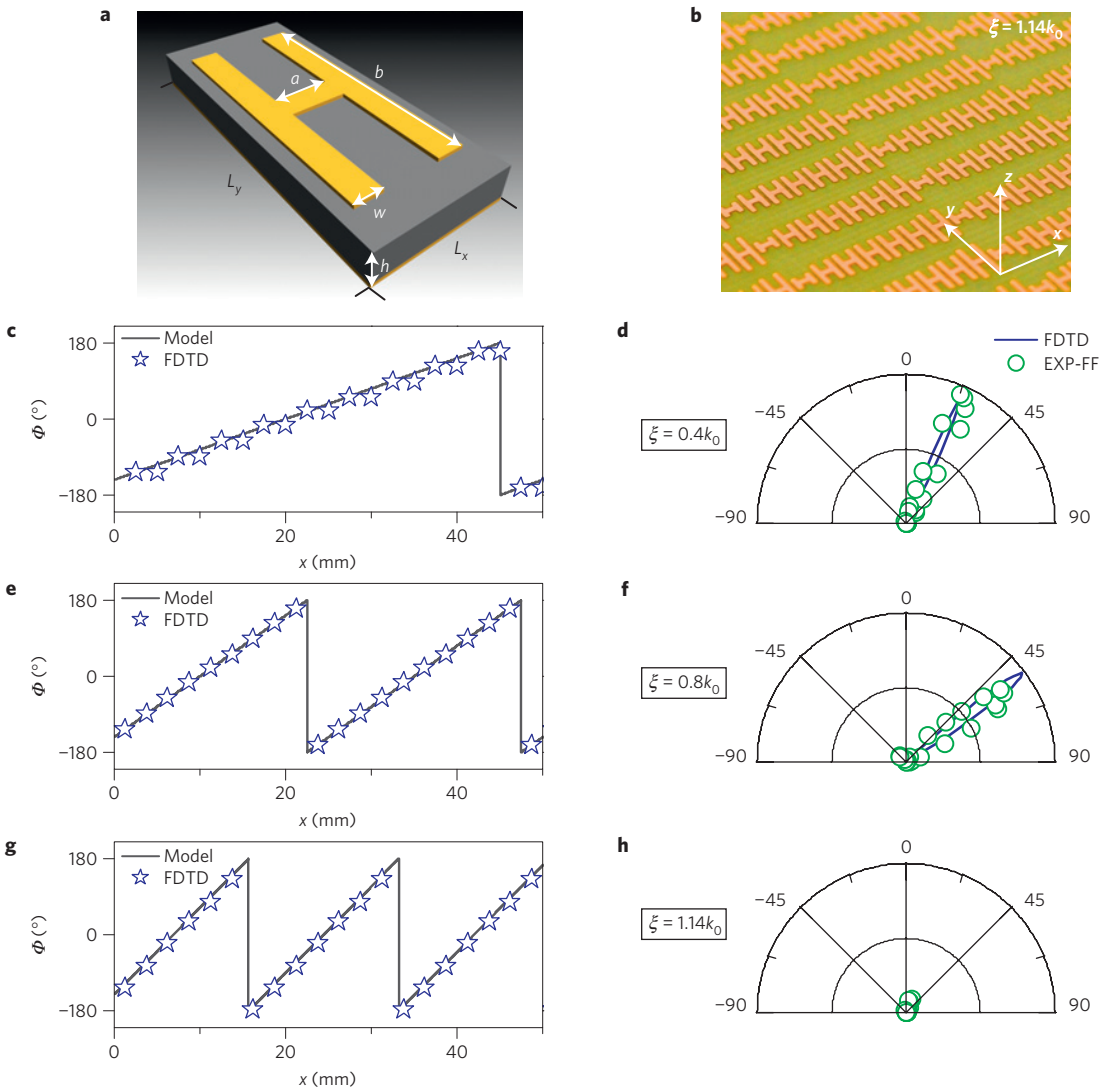

Figure 2 | Sample design, fabrication, and far-field characterization. a, The building block of our design consists of a metallic 'H' and a metal plate separated by a dielectric spacer ($\varepsilon = 3.9$). Parameters L_x, L_y, a, w, h are fixed as 2.5 mm, 6 mm, 1 mm, 0.5 mm and 1 mm, respectively, in all designs, while b changes within a super cell with the details recorded in Supplementary Information. **b**, Picture of part of the fabricated $\xi = 1.14k_0$ sample. **c**–**h**, Reflection phase distributions $\Phi(x)$ (**c**,**e**,**g**), and measured and simulated scattering patterns (**d**,**f**,**h**) for three meta-surfaces with $\xi/k_0 = 0.4, 0.8$ and 1.14.

(that is, both incident and reflected beams are PWs), and such a phenomenon can also be realized by the reflectarrays/transmitarrays in microwave engineering[33]. However, a significant new discovery here is that our meta-surface can further link a PW with a SW with nearly 100% efficiency, which is not noted in previous works.

Our ideas can be realized in any frequency regime as long as the model systems can be designed and fabricated. As a proof of concept, here we choose the microwave regime to verify our ideas. As shown in Fig. 2a, the building block of our design consists of a metallic 'H' and a metal sheet, separated by a dielectric spacer. Coupling between two metallic sheets generates a magnetic resonance so that the entire system can be modelled by a MM with particular ε, μ located on top of a perfect metal[34]. Choosing the working frequency as $f = 15$ GHz, we successfully designed and fabricated three gradient-index meta-surfaces with $\xi/k_0 = 0.4, 0.8, 1.14$. A picture of part of fabricated $\xi = 1.14k_0$ sample is shown in Fig. 2b. To justify our designs, we employed finite-difference-time-domain (FDTD) simulations to calculate the local reflection-phase distributions $\Phi(x)$ for all three samples, and Fig. 2c,e and g verify that equation (3) holds well for all samples with the desired ξ values. Illuminating these meta-surfaces with normally incident x-polarized EM waves, we measured the far-field (FF) scattering patterns and show the normalized patterns in Fig. 2d,f and h for three samples, correspondingly. We can easily identify the scattering maxima at $\theta_r = 23°$ and $\theta_r = 53°$ for the $\xi = 0.4k_0$ and $\xi = 0.8k_0$ cases, agreeing well with FDTD simulations performed on realistic structures. Intriguingly, for the $\xi = 1.14k_0$ sample, both FF experiment and FDTD simulation failed to detect any scattered FF signals, as can be seen in Fig. 2h.

To explore what happens in the $\xi = 1.14k_0$ case, we adopted a near-field (NF) scanning technique[3,6] to map the local field distribution on the meta-surface, with experimental set-up schematically described in Fig. 3a. Figure 3b shows the measured E_z-field distribution (with phase information included) on part of the $\xi = 1.14k_0$ meta-surface under illumination by a normally incident PW. The FDTD simulated pattern is shown in Fig. 3c, which is in excellent agreement with the measured pattern. We identify from the patterns that the E_z distribution does exhibit a well-defined parallel **k** vector $k_x \approx 1.14k_0$, which is identical to ξ. This fact tells us that the EM wave 'reflected' by the $\xi = 1.14k_0$ meta-surface can not leave the surface, and becomes a SW trapped by the meta-surface because

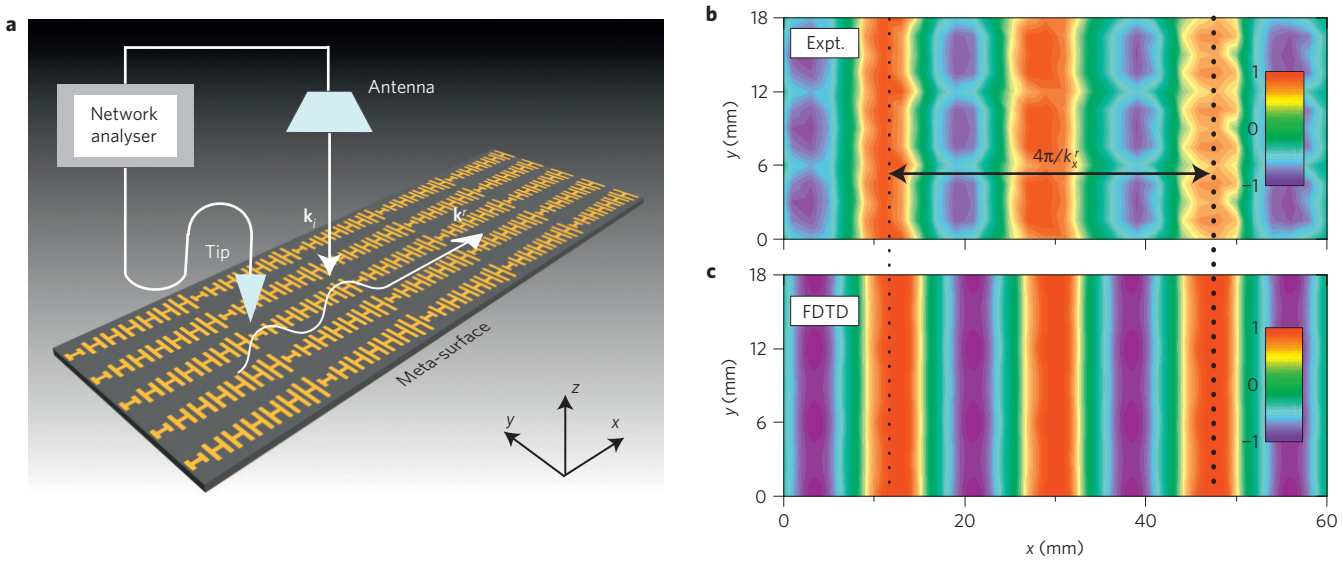

Figure 3 | Near-field characterizations on the meta-surfaces. a, Schematic picture describing the near-field scanning technique. **b**,**c**, E_z distributions (with phase information included) on part of the $\xi = 1.14k_0$ meta-surface under illumination of a normally incident *x*-polarized EM wave, obtained by near-field scanning measurements (**b**) and FDTD simulations (**c**).

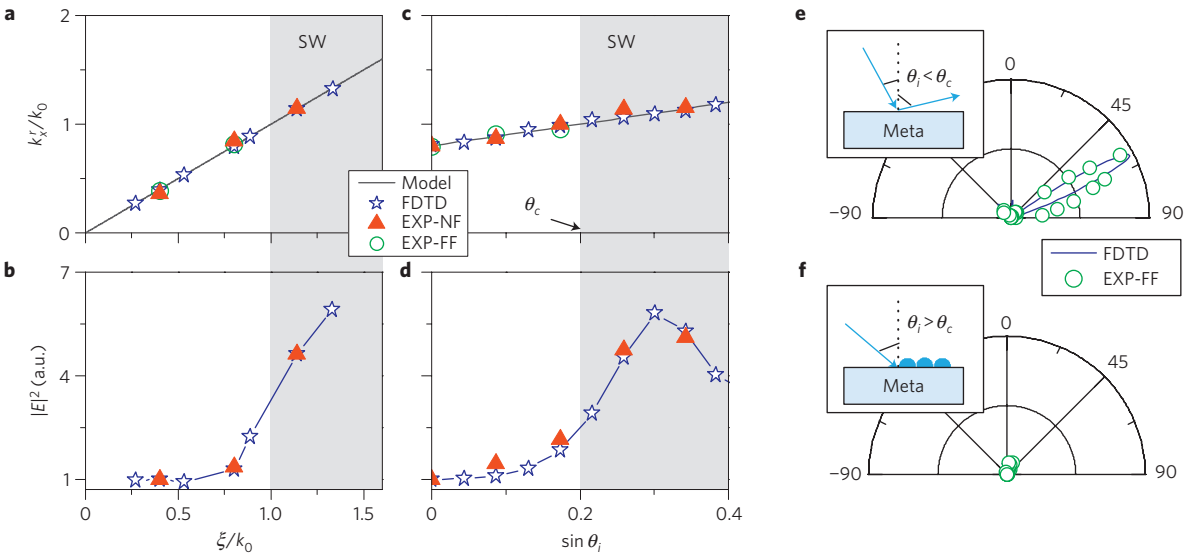

Figure 4 | Verifications of the dispersion relation $k_x^r = \xi + k_0 \sin\theta_i$. a,**b**, For meta-surfaces with different ξ/k_0 illuminated by the same normally incident *x*-polarized wave, measured (including FF and NF) and simulated parallel **k** vectors (k_x^r) of the waves generated by the meta-surfaces (**a**), and the normalized **E** field of the hot-spot on those meta-surfaces (**b**), as functions of ξ/k_0. Solid line in **a** represents the relation $k_x^r = \xi$. **c**,**d**, For the $\xi = 0.8k_0$ meta-surface, measured (including FF and NF) and simulated parallel **k** vectors (k_x^r) of the waves generated by the system (**c**), and the normalized **E** field of the hot-spot on its surface (**d**), as functions of θ_i at which a p-polarized beam ($\mathbf{H} \parallel \hat{\mathbf{y}}$) is incident on the meta-surface. Solid line in **c** represents the relation $k_x^r/k_0 = 0.8 + \sin\theta_i$. **e**,**f**, Measured and simulated FF scattering patterns generated by the $\xi = 0.8k_0$ meta-surface, when illuminated by a p-polarized beam ($\mathbf{H} \parallel \hat{\mathbf{y}}$) at incident angle $\theta_i = 5° < \theta_c$ (**e**) and $\theta_i = 25° > \theta_c$ (**f**). Here $\theta_c = \sin^{-1}(0.2) \approx 12°$.

$k_x > k_0$, which explains why the FF measurement failed to detect any signals (Fig. 2h).

Using such a NF scanning technique, we further measured the parallel **k** vectors (k_x^r) from the surface E_z distributions on meta-surfaces with $\xi = 0.4k_0$ and $\xi = 0.8k_0$, under the illumination of the same input beam. The obtained k_x^r are plotted in Fig. 4a as solid triangles. We also used the formula $k_x^r = k_0 \sin\theta_r$ to retrieve k_x^r from the measured FF scattering patterns (Fig. 2d,f) and plot the obtained data in Fig. 4a as open circles. Finally, in addition to three fabricated samples, we designed four meta-surfaces with $\xi/k_0 = 0.27, 0.53, 0.89, 1.33$, and performed FDTD simulations to calculate the values of k_x^r for all seven meta-surfaces under the illumination of the same input beam. The FDTD results are shown in the same figure as open stars. All the data, from the FF and NF experiments as well as FDTD simulations, fall onto one line $k_x^r = \xi$, which is just equation (4) with $\theta_i = 0°$ (normal-incident input). As an independent check, we show in Fig. 4b both the measured and simulated maximum local **E** field on the surfaces of different samples when illuminated by input waves with the same power. Both experiments and simulations show that the local **E** field is obviously enhanced on the sample(s) with $\xi/k_0 > 1$, reinforcing the generation of SWs on such meta-surfaces.

Equation (4) indicates that the incident angle θ_i is another parameter to determine k_x^r. Taking the $\xi = 0.8k_0$ sample as

an example, we performed both experiments (FF and NF) and FDTD simulations to verify this prediction. As shown in Fig. 4c, the measured and simulated data show that the relation $k_x^r/k_0 = \sin\theta_i + 0.8$ holds perfectly well. In particular, we found a critical value $\theta_c = \sin^{-1}(0.2) \approx 12°$ for θ_i, above which the beam reflected by the $\xi = 0.8k_0$ meta-surface disappears at the far field (Fig. 4e,f). Meanwhile, Fig. 4d shows that the local field on the meta-surfaces is obviously enhanced as $\theta_i > \theta_c$, again implying the generation of SWs.

Figure 4 reveals the key difference between our findings and conventional PW–SW conversion rendered by prism[23] or grating[24–26] couplers. The latter are based on resonant coupling between PW and SW and thus a high conversion efficiency can only happen for one particular θ_i where the momenta match. In contrast, our device can covert any PW with $\theta_i > \theta_c$ completely to a SW bounded on the meta-surface, and thus the bridging between PW and SW is much more robust and flexible (see Supplementary Information).

Different from surface plasmon polaritons (SPPs), which are the eigen EM surface modes of a given system, here the SWs are driven by incident PWs and can only flow on the meta-surfaces under the illumination of certain PWs. However, we show below that such 'driven' SWs can be guided out to SPPs on other systems. It has been experimentally proven that a mushroom structure supports SPP-like eigen EM modes in the microwave regime[35]. Therefore, we designed and fabricated an appropriate mushroom structure (see Supplementary Information) and directly attach it to our $\xi = 1.14k_0$ meta-surface. Illuminating only the meta-surface with a normally incident x-polarized microwave at 15 GHz, we performed a NF experiment to measure the field distributions on both the meta-surface and the mushroom surface (Fig. 5a). Both the NF experiment (Fig. 5b) and FDTD simulation (Fig. 5c) show that the SW generated on the meta-surface can indeed be guided out to flow on the mushroom as a SPP. As a control experiment, we repeated the measurements after replacing the meta-surface by a flat metal sheet, but found no SPP signals on the mushroom surface. We note that such a SW–SPP coupling scheme does not require strict momentum matching (that is, $\lambda_{SW} = \lambda_{SPP}$), and thus the coupling seems rather robust and flexible (see Supplementary Information).

In summary, we demonstrated that a gradient-index meta-surface is the very bridge to link PWs and SWs. Besides obvious interest in fundamental science, our findings may lead to many practical applications. For example, the high PW–SW conversion efficiency can be used to make a surface plasmon coupler; the complete suppression of specular reflections is useful in anti-reflection and invisibility applications; redirecting a PW to bounded SWs can be very helpful in light absorption applications. Although we only show the results at 15 GHz in the main text, the working bandwidth of the noted phenomena is about 1 GHz (see Supplementary Information) and can be further enlarged if non-resonant high-index materials are used. We believe that realizing these ideas, particularly at high frequencies, is exciting and challenging for future projects.

Methods

Theory and simulations. The $|\rho_{k_x}|^2$ spectra shown in Fig. 1d and f were calculated by the mode-expansion theory, of which details of the theoretical development are described in the Supplementary Information. Numerical simulation results shown in Figs 2–5 were obtained by FDTD simulations using a numerical solver (CONCERTO 7.0, Vector Fields Limited, UK(2008)). Absorbing boundary conditions are implemented to remove the energy of those SWs flowing outside the simulation domain and a small dielectric loss is adopted to make the simulations converge fast.

Sample fabrication. All samples were fabricated using 1.0-mm-thick FR4 printed circuit boards with one side covered by a 35-μm-thick continuous copper film and the other side covered with copper patterns etched based on the theoretical designs.

Characterizations. In the FF experiments, the incident EM waves were generated by a horn antenna placed 2 m away from the samples, and the scattering patterns were measured with another identical horn antenna, which was placed at the same distance and could be freely moved around the sample. Both antennas were corrected to a vector network analyser (Agilent E8362C PNA). The received signals were normalized against a reference measured when the meta-surface was replaced by a metal plate of the same size. In the NF experiments, illuminating the meta-surfaces with a horn antenna placed 2 m away, a 1.5 cm long monopole antenna was placed at a 1 mm distance from the meta-surfaces to measure both the amplitudes and phases of the received signals. Both antennas were connected to a vector network analyser (Agilent E8362C PNA). The monopole antenna was placed perpendicular to the surface so that it mainly coupled to the local E_z field on the surface. Figure 3 shows the real part of the measured field, representing the instantaneous field pattern at a particular time. All data are normalized with respect to that for $\xi = 0.4k_0$ in Fig. 4b and to that for $\theta_i = 0°$ in Fig. 4d.

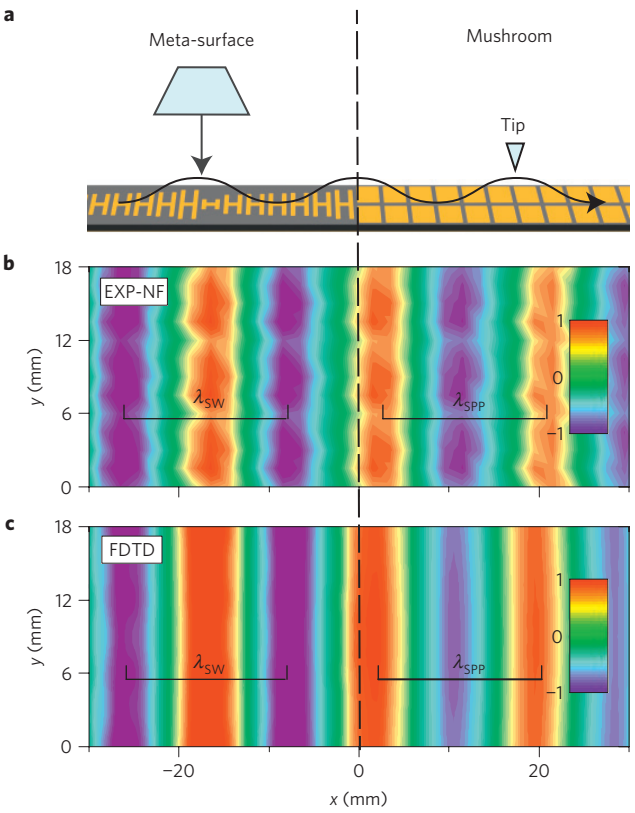

Figure 5 | Guiding the driven SWs outside the meta-surface. a, Schematics of the experimental set-up. **b**,**c**, E_z distribution (with phase information included) on both the $\xi = 1.14k_0$ meta-surface and the mushroom surface, obtained by NF experiments (**b**) and FDTD simulations (**c**) at 15 GHz.

Received 7 October 2011; accepted 2 March 2012; published online 1 April 2012

References

1. Leonhardt, U. Optical conformal mapping. *Science* **312,** 1777–1780 (2006).
2. Pendry, J. B., Schurig, D. & Smith, D. R. Controlling electromagnetic fields. *Science* **312,** 1780–1782 (2006).
3. Schurig, D. *et al.* Metamaterial electromagnetic cloak at microwave frequencies. *Science* **314,** 977–980 (2006).
4. Cai, W. S., Chettiar, U. K., Kildishev, A. V. & Shalaev, V. M. Optical cloaking with metamaterials. *Nature Photon.* **1,** 224–227 (2007).
5. Chen, H. Y., Chan, C. T. & Sheng, P. Transformation optics and metamaterials. *Nature Mater.* **9,** 387–396 (2010).
6. Ma, H. F. & Cui, T. J. Three-dimensional broadband ground-plane cloak made of metamaterials. *Nature Commun.* **1,** 21 (2010).
7. Liu, Y. M., Zentgraf, T., Bartal, G. & Zhang, X. Transformational plasmon optics. *Nano Lett.* **10,** 1991–1997 (2010).
8. Huidobro, P. A., Nesterov, M. L., Martin-Moreno, L. & García-Vidal, F. J. Transformation optics for plasmonics. *Nano Lett.* **10,** 1985–1990 (2010).
9. Aubry, A. *et al.* Plasmonic light-harvesting devices over the whole visible spectrum. *Nano Lett.* **10,** 2574–2579 (2010).

10. Zentgraf, T., Liu, Y. M., Mikkelsen, M. H., Valentine, J. & Zhang, X. Plasmonic Luneburg and Eaton lenses. *Nature Nanotech.* **6,** 151–155 (2011).
11. Tsakmakidis, K. L., Boardman, A. D. & Hess, O. 'Trapped rainbow' storage of light in metamaterials. *Nature* **450,** 397–401 (2007).
12. Gan, Q. Q., Fu, Z., Ding, Y. J. & Bartoli, F. J. Ultrawide-bandwidth slow-light system based on THz plasmonic graded metallic grating structures. *Phys. Rev. Lett.* **100,** 256803 (2008).
13. Levy, U. *et al.* Inhomogenous dielectric metamaterials with space-variant polarizability. *Phys. Rev. Lett.* **98,** 243901 (2007).
14. Pinchuk, A. O. & Schatz, G. C. Metamaterials with gradient negative index of refraction. *J. Opt. Soc. Am. A* **24,** A39–A44 (2007).
15. Paul, O., Reinhard, B., Krolla, B., Beigang, R. & Rahm, M. Gradient index metamaterial based on slot elements. *Appl. Phys. Lett.* **96,** 241110 (2010).
16. Kundtz, N. & Smith, D. R. Extreme-angle broadband metamaterial lens. *Nature Mater.* **9,** 129–132 (2010).
17. Vasić, B., Isić, G., Gajić, R. & Hingerl, K. Controlling electromagnetic fields with graded photonic crystals in metamaterial regime. *Opt. Express* **18,** 20321–20333 (2010).
18. Smith, D. R., Mock, J. J., Starr, A. F. & Schurig, D. Gradient index metamaterials. *Phys. Rev. E* **71,** 036609 (2005).
19. Lin, X. Q. *et al.* Controlling electromagnetic waves using tunable gradient dielectric metamaterial lens. *Appl. Phys. Lett.* **92,** 131904 (2008).
20. Liu, R. *et al.* Broadband gradient index microwave quasi optical elements based on non-resonant metamaterials. *Opt. Express* **17,** 21030–21041 (2009).
21. Yu, N. *et al.* Light propagation with phase discontinuities: Generalized laws of reflection and refraction. *Science* **334,** 333–337 (2011).
22. Ni, X., Emani, N. K., Kildishev, A., V., Boltasseva, A. & Shalaev, V. M. Broadband light bending with plasmonic nanoantennas. *Science* **335,** 427 (2012).
23. Kretschmann, E. & Raether, H. Radiative decay of nonradiative surface plasmons excited by light. *Z. Naturforsch.* **23A,** 2135–2136 (1968).
24. Raether, H. *Surface Plasmons on Smooth and Rough Surfaces and on Gratings* (Springer, 1988).
25. Neviere, M., Petit, R. & Cadilhac, M. About the theory of optical crating coupler-waveguide systems. *Opt. Commun.* **8,** 113–117 (1973).
26. Tang, Y. B., Wang, Z. C., Wosinski, L., Westergren, U. & He, S. L. Highly efficient nonuniform grating coupler for silicon-on-insulator nanophotonic circuits. *Opt. Lett.* **35,** 1290–1292 (2010).
27. Barnes, W. L., Dereux, A. & Ebbesen, T. W. Surface plasmon subwavelength optics. *Nature* **424,** 824–830 (2003).
28. Born, M. & Wolf, E. *Principles of Optics: Electromagnetic Theory of Propagation, Interference and Diffraction of Light* (Cambridge Univ. Press, 1999).
29. Grüner, G. The dynamics of charge-density waves. *Rev. Mod. Phys.* **60,** 1129–1181 (1988).
30. Landau, L. D., Liftshitz, E. M. & Pitaevskii, L. P. *Electrodynamics of Continuous Media* 2nd edn (Pergamon, 1984).
31. Sheng, P., Stepleman, R. S. & Sanda, P. N. Exact eigenfunctions for square-wave gratings: Application to diffraction and surface-plasmon calculations. *Phys. Rev. B* **26,** 2907–2917 (1982).
32. Garcia-Vidal, F. J., Martín-Moreno, L. & Pendry, J. B. Surfaces with holes in them: New plasmonic metamaterials. *J. Opt. A Pure Appl. Opt.* **7,** S97–S101 (2005).
33. Bansal, R. Bending Snell's laws. *IEEE Antenn. Propag. Mag.* **53,** 146–147 (2011).
34. Hao, J. M., Zhou, L. & Chan, C. T. An effective-medium model for high-impedance surfaces. *Appl. Phys. A* **87,** 281–284 (2007).
35. Lockyear, M. J., Hibbins, A. P. & Sambles, J. R. Microwave surface-plasmon-like modes on thin metamaterials. *Phys. Rev. Lett.* **102,** 073901 (2009).

Acknowledgements

This work was supported by the National Natural Science Foundation of China (60990321, 11174055, 60725417) and the Ministry of Education of China (B06011). S.S. was supported by the National Science Council and National Center for Theoretical Sciences of Taiwan. We thank Y. R. Shen and C. T. Chan for helpful discussions.

Author contributions

S.S. did the theoretical calculations and designed the samples. Q.H. and S.X. made the samples and did the measurements. Q.X. helped in theoretical calculations. X.L. helped in experimental measurements. L.Z. conceived the idea, developed the mode-expansion theory and wrote the manuscript.

Additional information

The authors declare no competing financial interests. Supplementary information accompanies this paper on www.nature.com/naturematerials. Reprints and permissions information is available online at www.nature.com/reprints. Correspondence and requests for materials should be addressed to L.Z.